Control of thermocapillary instabilities far from threshold

P. Brunet,[a] G. Amberg, and P. H. Alfredsson
KTH Mechanics, SE-10044 Stockholm, Sweden

(Received 3 March 2005; accepted 13 September 2005; published online 25 October 2005)

We report experiments on control of thermocapillary instabilities at high temperature differences, in an annular geometry. Previous studies [Phys. Fluids **14**, 3039 (2002)] showed that a reasonable control of oscillatory instability could be achieved by optimizing a local heating feedback process. We conducted experiments with a basic flow converging from periphery to center. This constitutes a more unstable configuration than previously, and enables appearance of higher-order instabilities and chaos. Applying successfully local feedback control to the periodic state close to the threshold, we extend the process to higher temperature differences, where nonlinear as well as proportional/derivative control laws are necessary to obtain a significant decrease of the temperature fluctuations. Finally, proportional control allows us to synchronize a chaotic state, to a periodic one. © *2005 American Institute of Physics*. [DOI: 10.1063/1.2111144]

I. INTRODUCTION

Thermocapillary driven flows appear in a large class of systems in everyday's life and practical applications, where a nonhomogeneous heating on a free surface is involved. This can be encountered in manufacturing of crystals using float-zone methods or in welding operations. The basic flow is caused by tangential stresses due to dependence of surface tension upon temperature, which leads to large-scale fluid motion as a consequence of convection and mass conservation. This is known as Bénard-Marangoni convection. Recently, it has been shown that such a flow can prevent the dripping of a hanging drop by counterbalancing the gravity-driven Rayleigh-Taylor instability.[1] When the liquid surface is flat, no gravity effect opposes the thermocapillary flow and this latter appears as soon as the tiniest temperature gradient is applied. This is reviewed in Ref. 2 in which one finds predictions for further bifurcations that would occur above larger temperature gradients. An oscillatory regime with a rotating wave was indeed observed[3] in a cylindrical container of an aspect ratio of approximately one, at a moderate (around 20) Prandtl number (Pr). Several other studies have been conducted under similar experimental conditions,[4–6] which revealed the appearance of complexity, in temporal signal fluctuations as well as in spatial structures, the latter being strongly influenced by the aspect ratio. In particular, these studies have shown a clear dependency of the aspect ratio on the dominant spatial mode: the smallest the aspect ratio, the highest the dominant wave number. The simplest spatial structures (an azimuthal wave number of 2 or 3) are then obtained with aspect ratios around one.

Focusing on practical purposes, the flow dynamics of the cylindrical-container geometry studied in Ref. 3 mimics the one of the floating-zone geometry involved in production of single crystals, where oscillatory instabilities lead to striation in the final product.[7] For a more complete presentation of the floating-zone geometry (and the closely related half-zone), see Refs. 8–10, and references therein. Although recent experiments with floating zones have been conducted under microgravity conditions to prevent imperfect lateral surface deformations,[11] the cylindrical geometry diminishes the influence of gravity, providing that the container is small enough. Let us mention that microgravity experiments were also conducted in cylindrical containers.[12] Some of these studies also mentioned the existence of oscillatory instabilities as a first step toward more complex dynamics, that it would be necessary to control in order to obtain purer crystals.

Recently, several studies have been conducted to that purpose, in a cylindrical container on which the temperature gradient is applied from the center to the periphery[13] and in a half-zone liquid bridge:[10] it was experimentally shown that oscillations could be controlled by a simple feedback scheme involving local heating on the surface. Due to the constrained geometry and the close-to-one aspect ratio, the spatial structure of the flow is simple and allows the use of only a few heaters (typically one, two, or three). Some theoretical attempts addressed this problem in a slightly different geometry—a layer of liquid heated from below.[14,15] It is shown that a linear feedback enables one to delay the threshold of primary instability. This was indeed experimentally shown in Ref. 13 where a linear scheme was found to be sufficiently close to the onset of oscillations, and that nonlinear control becomes necessary when the system is driven further from the threshold. The question that should then naturally arise is—could such a control be conducted for larger temperature differences, when the flow undergoes more complex dynamics approaching chaos? However, until now, it was not possible to observe further secondary instabilities and chaos beyond the oscillatory instability in the annular geometry. One of the limitations of previous experiments was that beyond a certain temperature difference, bubbles and evaporation occurred, and dramatically perturbated the flow. Inspired by a recent study that emphasized the influence of reversing temperature,[11] it is presented in this article that it is possible to obtain complex flow dynam-

[a]Electronic mail: brunet@mech.kth.se

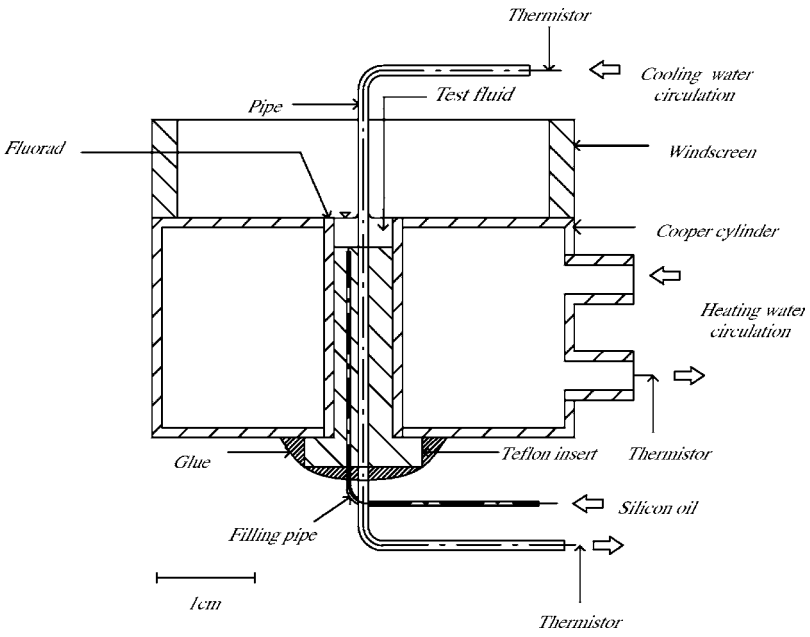

FIG. 1. Experimental setup.

ics, and reported control of such states far from the onset. The converging flow obtained in this configuration, is more unstable than the diverging flow studied before,[13] allowing the occurrence of chaos for reasonable temperature differences.

In the last three decades, considerable efforts have been developed to understand the appearance of unpredictable dynamics in geometrically confined systems,[16] and a further step was to investigate how to achieve stabilization of these complex behaviors. The pioneering paper by Ott *et al.*[17] showed that a suitable control could be achieved by applying small, optimal perturbations, in order to drive the system to a periodic attractor. Optimization is determined during an initial phase, when the control algorithm "learn" how the system reacts to model perturbations. This can be costly in computation and complex to implement in real experimental situations, and for that reason this method was restricted to spatially constrained systems. This was successfully applied to control oscillating states in a liquid-bridge experiment.[18] Another example of such successful control was achieved in a thermal convection loop exhibiting two-state intermittent chaos, by Bau and co-workers.[19–21] In the study reported here, a more simple feedback control scheme is used, based on local measurements of temperature near the surface. Such a control leads to a significant decrease of temperature fluctuations far from the oscillatory bifurcation threshold (even efficient when the first steps of further bifurcations occur), as well as synchronization of chaos to a periodic state, at a very high temperature difference. The temperature difference may be expressed in a nondimensional form as

$$\epsilon = \frac{\Delta T - \Delta T_c}{\Delta T_c}, \tag{1}$$

when ΔT is the temperature difference applied between the periphery and the center of the cell, and ΔT_c is the temperature difference at the oscillatory threshold. In our setup, it is possible to conduct experiments up to $\epsilon = 1.9$ if the hot temperature is applied on the periphery. Beyond this value, bubbles occur anyway as a consequence of liquid evaporation. The control is found to be relatively efficient up to ϵ around 1. In this article, we explore control strategies in more complex dynamics flow regimes.

Such a study has two purposes as to propose issues for a practically puzzling situation of crystal deterioration and as to conduct feedback control on a relatively simple system, the dynamics of which is generically described by a set of Ginzburg-Landau-like amplitude equations, at least not too far from threshold. Further, studying the reaction of an unstable system under applied control, can give information about its sensitivity to small perturbations as well as the vicinity of different unstable regimes from attraction basins.

In the following, we first detail the experimental setup (Sec. II), then we give information of the flow structure without control at increasing ϵ (Sec. III). In Sec. IV we show results of controlled dynamics for moderate ϵ, where the flow regime is oscillatory. Section V reports some results of successful control at higher ϵ, with a control law which includes a derivative term. Section VI presents synchronization of a chaotic regime to simple oscillatory dynamics, achieved by the same kind of feedback law. Section VII then gives a summary of results and presents our conclusions.

II. EXPERIMENTAL SETUP

With the exception of the reverse of the temperature gradient, the experimental setup is the same as that used in Ref. 13 where more details are given. The annular geometry consists of a cylindrical container with a small coaxial cylindrical cooler. A thermocapillary convection in an open cylindrical container filled with silicone oil, Pr=14 at 25 °C, is driven by imposing a radial temperature gradient on the horizontal free surface. In Fig. 1, the experimental setup is presented. Figure 2(a) shows a sketch of both the annular configuration and the two-dimensional steady flow.

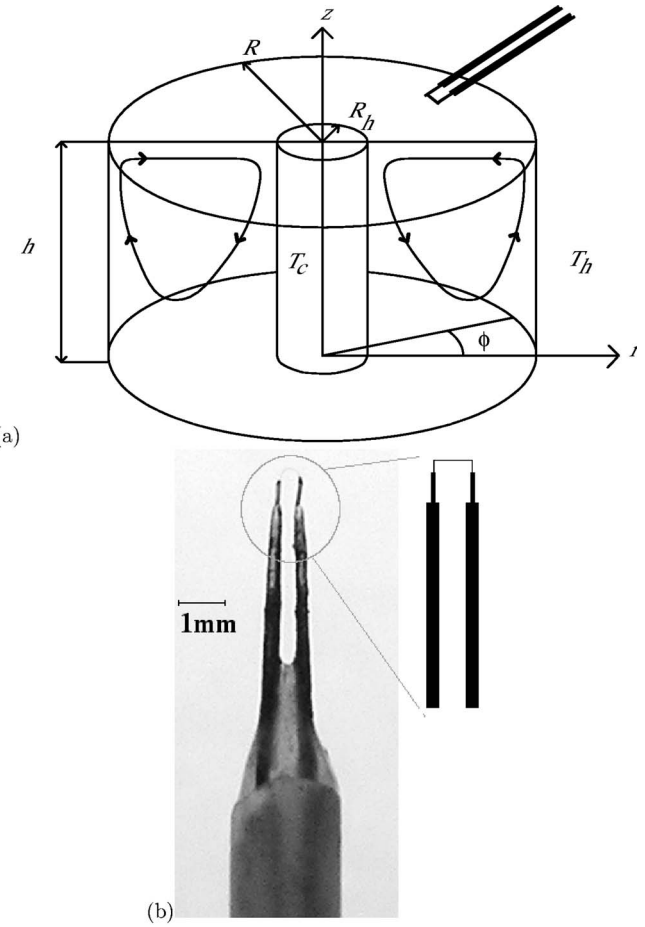

FIG. 2. (a) Sketch of the steady flow, with a sensor and (b) close-up of one of the sensors/heaters, and further close-up.

The test fluid is contained in a copper cylinder of an inner radius $R=3$ mm. Coaxial with the cylinder, there is a pipe made of stainless steel of a radius $R_h=0.63$ mm that acts as a central cooler. A copper cylinder which acts as an outside wall is surrounded by the heating tank. Two temperature boundary conditions are set to impose the temperature gradient; one by circulating cold water through the pipe and the other by circulating warm water through the tank. The aspect ratio $A_r=R/h$ is kept at unity. The ratio of the radius of the pipe R_h to R is $H_r=0.21$. At this A_r, the dominant azimuthal wave number (mode) of the oscillatory state is known to be 2 or 3. The choice of 1 cSt silicone oil is a result of a compromise between volatility and required temperature difference for the instabilities. Silicone oil with lower viscosity is too volatile whereas, with higher viscosity, the required temperature gradient is difficult to be reached with the current experimental setup. Since evaporation to some extent is inevitable, the evaporation was compensated by continuously adding a small volume of liquid to the cell through a tiny hole on the bottom connected to a relatively larger cylinder filled with the same liquid. An insulating insert made of Teflon was used to provide a near adiabatic boundary condition at the bottom of the cell.

The essential modification from the previous studies,[13] is that the hot and the cold temperatures have been reversed: the radial temperature gradient produced is such that the basic flow is driven from the periphery to converge to the center of the cell. One of the noticeable consequences induced by the converging geometry is that it is not possible to pin the free surface on a step on the small coaxial cooler: this was previously achieved with the diverging flow[13] by covering the small step on the cooler with a layer of weak surface energy (Fluorad). With the converging geometry, the pinning of the surface cannot be maintained, presumably because of a more violent flow. We then use a simple vertical cylindrical cooler without step, which leads to a small meniscus due to capillary rising. This meniscus could affect the bifurcation to oscillatory states,[2] making it imperfect. Nevertheless, this drawback is not of first importance, considering that our study focuses on phenomena far from the threshold. Further, the silicone oil perfectly wets the central cooler, and this rejects the possibility of a contact angle hysteresis which could imply unrepeatable experiments. Special care has been thus devoted to check the repeatability of the flow, for example by measuring amplitude of oscillatory states day to day.

The Marangoni number, quantifying the ratio between capillary driving forces and viscous damping, is defined as

$$\mathrm{Ma}=\frac{\gamma\Delta TR}{\mu\alpha}, \tag{2}$$

where $\Delta T=T_h-T_c$, and γ, α, and μ are the surface tension coefficient, thermal diffusivity and dynamic viscosity, respectively. T_h and T_c are the temperatures of the hot and cold walls and Ma is the relevant number to quantify the value of different thresholds for successive bifurcations. However, for sake of clarity, and because the value of the critical Marangoni number for appearance of oscillations is of the order of 40 000, we use instead the quantity ϵ defined in Eq. (1).

The sensors (measuring local temperature) and heaters (injecting feedback power) are U shaped wires which are made of platinum and 90%–10% platinum-rhodium, respectively. The diameter of these wires is 1 μm. The length of the heaters is $L_h=1.5$ mm, whereas sensors are much smaller $L_s=0.5$ mm [see Fig. 2(b)]. Their resistance at ambient temperature are approximately $R_{\mathrm{heater}}=60\ \Omega$ ($T\simeq 20\ ^\circ\mathrm{C}$) and $R_{\mathrm{sensor}}=12\ \Omega$ ($T\simeq 20\ ^\circ\mathrm{C}$). To prevent the heaters from being overloaded, the output voltage limit was set to be 3 V. In case the output signal exceeds the limit, the output voltage is given the limit value.

The radial position of the controllers is fixed at $r=R_h+(R-R_h)/2$. As for the vertical positions of the controllers, the sensors are installed through the free surface until the tip of the sensor is immersed to around 100 μm from the surface, whereas heaters are positioned above the surface. The probes are oriented to have the wires normal to the radial direction. The influence on the control of the distance between the free surface and the heaters was studied by testing the control for various distances from 25 to 450 μm. The results show that there is no influence in this range. Therefore, the distance of 50 μm was selected, which is equivalent to the one adopted in Ref. 13. We used two sensors and two heaters for our experiments. This choice is motivated by simplicity of the feedback scheme, taking into account that, as

will be seen below, the dynamics is dominated by a rotating spatial mode-2.

III. FLOW DYNAMICS WITHOUT CONTROL

Here is reported an overview of the different flow regimes at increasing temperature difference ΔT. Below a certain threshold ΔT_c, the flow is steady, axisymmetric, from periphery to center [Fig. 2(a)]. When ΔT is driven beyond ΔT_c, the flow undergoes a transition to an oscillatory regime which breaks the initial axial symmetry of the flow. A qualitative view of the flow could be observed, by seeding the liquid by light-reflective particles [flake-shaped particles of irodin 120 (TiO_2) of around 20 μm diam]. With these direct visualizations as well as with local temperature measurements presented thereafter, several facts can be emphasized:

- Just above the threshold, the oscillating regime shows an intermittent coexistence of two states of standing and traveling waves, which both have a spatial wave number of two to the azimuthal direction (this wave structure is denoted as "mode-2" in the following). The resulting temperature signal is a superimposition of these two periodic signals. This is named "Oscill T+S" in the following. This fact was also noticed in the divergent geometry.[13]
- At ϵ larger than around 0.15, the oscillatory flow-regime progressively becomes purely rotating (traveling wave), still of mode-2, named "Oscill T" in the sequel. Figure 3(a) shows the spatial structure of the dominant mode, as well as successive snapshots of the rotation obtained by image subtraction. At increasing ϵ, the amplitude of the wave increases. This mode is spatially different from the dominant one in the previously used diverging geometry:[13] the dimensionless wave number was there equal to 3, although an azimuthal mode-2 was already observed elsewhere also with diverging flow.[3] This is comparable to what is observed in the half-zone geometry, where occurrences of both mode-2 (Ref. 10) and mode-3 (Ref. 9) are observed.
- At ϵ larger than around 0.95, the periodic mode-2 state undergoes a further bifurcation with the appearance of a subharmonic mode. This leads to a time-period doubling, and constitutes the first step toward complexity, although the peak-to-peak temperature fluctuations do not evolve anymore.
- At ϵ larger than approximately 1.28, the flow enters a chaotic regime. The temperature fluctuations show suddenly very large bursts as well as moments of lower amplitude.

A schematic of the successive bifurcations is shown on Fig. 4. It should be pointed out that no sharp qualitative separation is observed when the flow goes from a T+S to a T regime, or from successive period-doubling states to chaos, and that the given value for ϵ at these boundaries are purely indicative.

As reported in Fig. 3(b), the amplitude of the oscillating mode A increases as the square root of the distance to threshold. Defining the dimensionless temperature θ as

$$\theta = \frac{T - \bar{T}}{\Delta T_c},$$

where $\bar{T}$ represents the mean value of T. This mean is evaluated from the signal, during the last 5 s, so that it evolves with time, in order to get rid of some slow fluctuations. The quantity A is measured as the square root if the value of the Fourier coefficient of the fundamental frequency in power spectra of θ. By extrapolating the amplitude to 0, ΔT_c is determined around 17 ± 0.3 °C. The corresponding Marangoni number is $\mathrm{Ma}_c = 44\,200 \pm 650$.

More careful observations of this oscillating regime reveal that the frequency does not evolve significantly with ϵ, and changes from 1.18 Hz at low ϵ to 1.25 Hz at higher ϵ. Small variations of the frequency was also observed for traveling waves in the half-zone geometry.[10]

Figures 5(a)–5(d) show evolution of the flow at increasing ϵ, with plots of extracted signal versus time, frequency power spectra and attractors built in a pseudophase space, in order to build a Poincaré map. These latter are obtained by simply plotting the quantities $T(t)$, $T(t+dt)$, and $T(t+2dt)$ for consecutive time steps. dt is taken equal to 1/20 s. The information that can be extracted from these plots witnesses what was briefly expressed before:

- At weaker ϵ (a), the local temperature has an oscillating behavior. The frequency power spectrum shows a dominant frequency around 1.2 Hz, and its first harmonics; the attractor is a simple loop corresponding to periodic oscillations.
- At higher ϵ (b), the period-doubling bifurcation is clearly witnessed, as new peaks rise in the spectrum, and the limit cycle is made of two loops. In the next set of plots (c), this tendency is even clearer, with appearance of other peaks. The attractor becomes smoother and smoother, although keeping a pseudoperiodic structure.
- At the highest ϵ (d), the flow is chaotic: the power spectrum does not show any sharp peak, but a smooth bump around 1.3 Hz. The time step for the Poincaré map dt is here taken equal to 1/35 s.

The chaotic spectra such as the one shown on Fig. 5(d), were obtained from long-time acquisitions (around 30 min) that were divided into a number of overlapping shorter samples (each 32 768 points, around 15 min) on which fast Fourier transform is applied. The resulting spectrum is then the average of all spectra and a running average (over eight points) is applied, which was found necessary to smooth the spectrum which otherwise has large meaningless variations.

Comparing to the liquid-bridge experiment, Ueno *et al.*[9] found in the latter system a more complex set of successive regimes. As in our observations, the transition towards chaos in the half-zone seems to exhibit the generic scenario of successive period doubling,[10] although no clear evidence of that could be found in Ref. 9. It is worth noticing that in another liquid-bridge experiment, a transition by quasi-periodicity, with the appearance of incommensurable frequencies and the

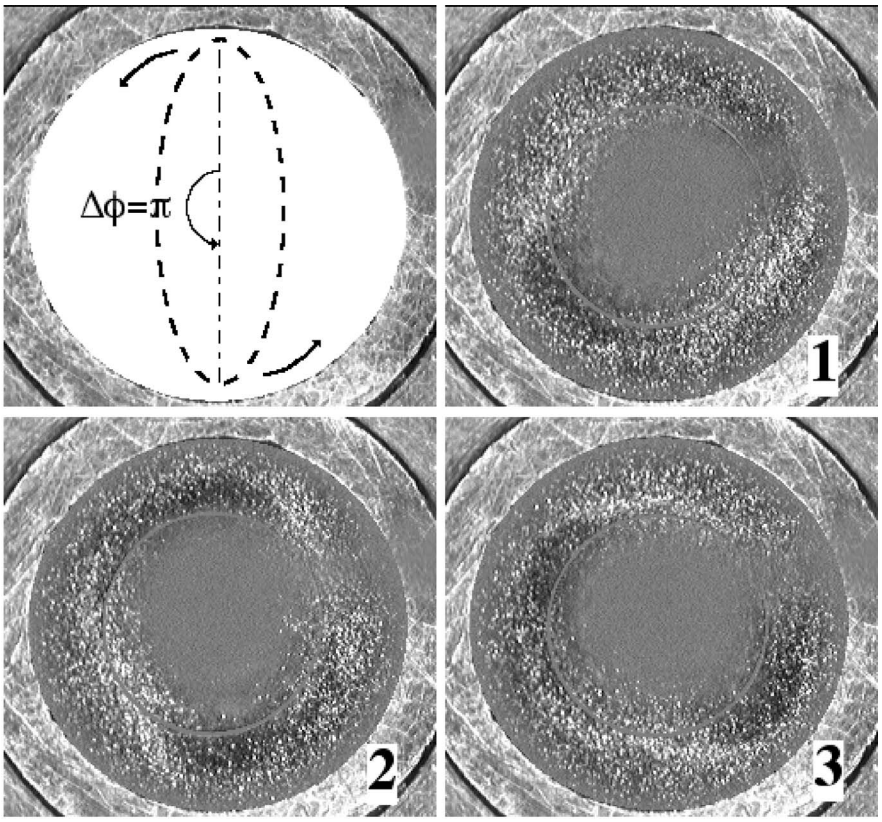

(a)

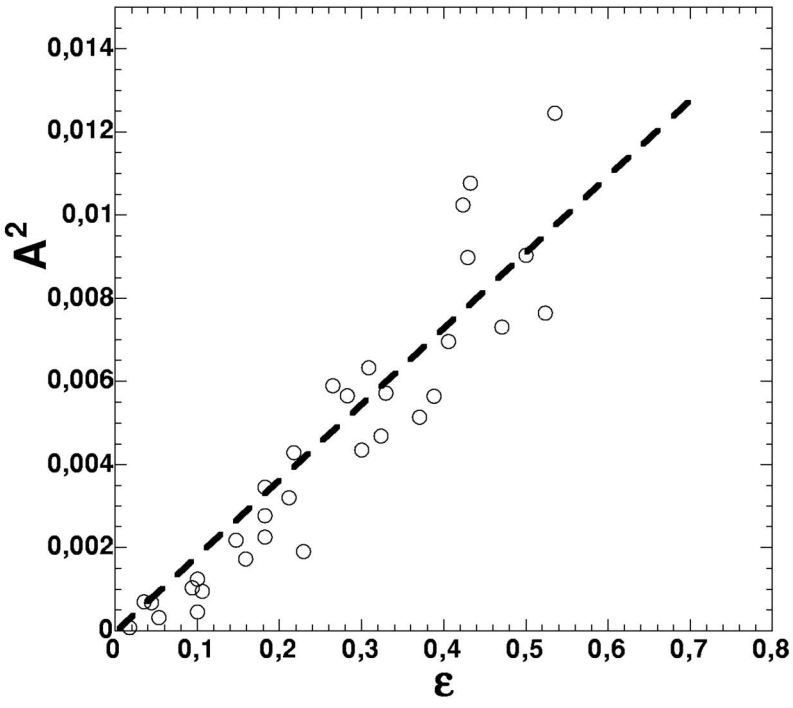

(b)

FIG. 3. (a) Spatial structure a traveling wave in the oscillating regime (top-left) of wave number 2, and three successive snapshots (time step=1/5 s) showing the rotating flow. The shadow circle represents light reflection on the not-perfect horizontal free-surface. (b) Amplitude of temperature fluctuations in an oscillating regime vs distance to threshold.

growth of a torus around the initial oscillatory attractor in the Poincaré map, was observed in Ref. 8. It is then difficult to conclude to a similar transition scenario in both cylindrical and half-zone geometry.

For a more quantitative evidence of transition to chaos, we calculated Lyapunov exponents by a method proposed in Ref. 22, and performed as well in Ref. 9. The principle of such calculation is to determine the mean distance versus

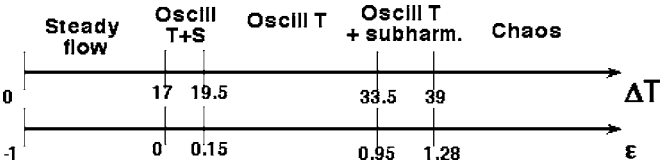

FIG. 4. Different steps of the flow regimes at increasing ΔT (see the text for details).

time between trajectories in the phase space, starting from two neighboring points. The value of the Lyapunov exponent is given by the divergence rate of the logarithm of the mean distance, versus time. Precisely, we take a set of n consecutive points $\mathbf{p}_n(\tau_0)$ starting at τ_0 from the time signal, as the reference point (lying then in a phase space of dimension n). Then we check the whole acquisition to determine if there exists points in the vicinity of the reference (in a sphere of radius ζ), measuring the distance between the reference set of n points and n other consecutive points of the acquisition (i.e., $|\mathbf{p}_n(\tau)-\mathbf{p}_n(\tau_0)|<\zeta$). When such a point is found $[\mathbf{p}_n(\tau_1)]$, we calculate the distance $|\mathbf{p}_n(\tau_1+t)-\mathbf{p}_n(\tau_0+t)|$ vs t.

For example, the Poincaré maps represent trajectories for $n=3$, but this value is far too small for such a calculation, as trajectories diverge quickly from each others in the three-dimensional phase space. We have chosen $n=50$ for samples, which corresponds to a duration of 1 s. The vicinity criterion ζ was chosen in order to obtain around a hundred of points that satisfy the criterion (during a 20 min acquisition). We run the calculation for 100 different reference samples. An example of the diverging mean distance versus time is plotted on Fig. 6(a), for a value of $\epsilon=1.67$. An exponential divergence can be measured during the first half-second (the value of the exponent is given by the slope of the dot-dashed line), whereas the distance grows slower afterwards. In chaotic regimes, exponents are found around 2 [Fig. 6(b)]. Acquisitions of oscillatory states show an exponential growth as well, but of much smaller rate and during more than 10 s. This is presumably due to the experimental noise and the slow variations of the mean signal. The close-to-zero corresponding values are plotted for comparisons, although they cannot be rigorously defined as Lyapunov exponents.

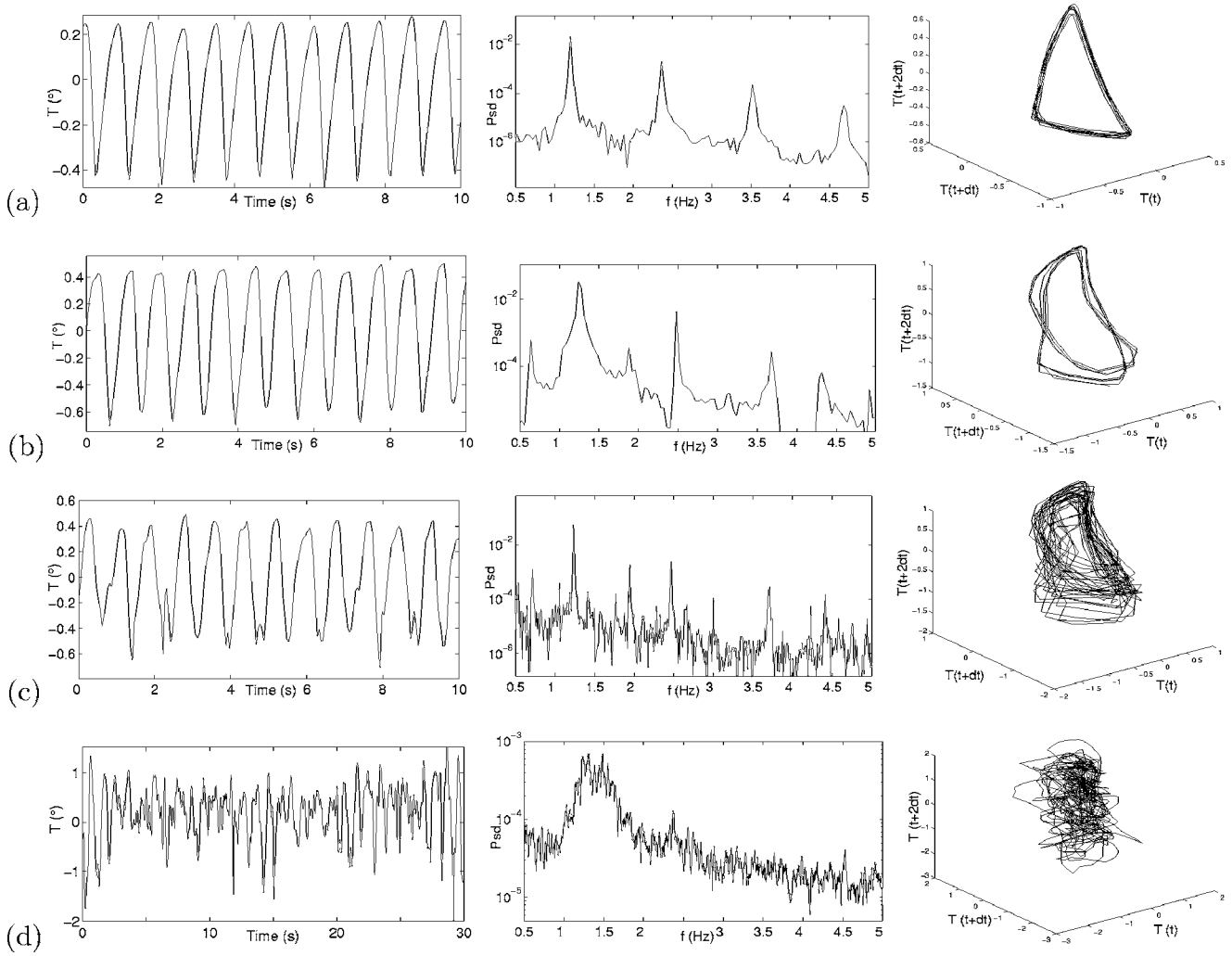

FIG. 5. Extracts of time signals, power spectra and reconstructed pseudophase space attractors (time step 1/20 s) for different increasing ΔT. (a) $\Delta T=26°$ ($\epsilon=0.53$): oscillatory regime; (b) $\Delta T=33.9°$ ($\epsilon=0.99$): period doubling; (c) $\Delta T=35.75°$ ($\epsilon=1.10$): further step to complexity; and (d) $\Delta T=47.6°$ ($\epsilon=1.8$): chaos. See the text for further details.

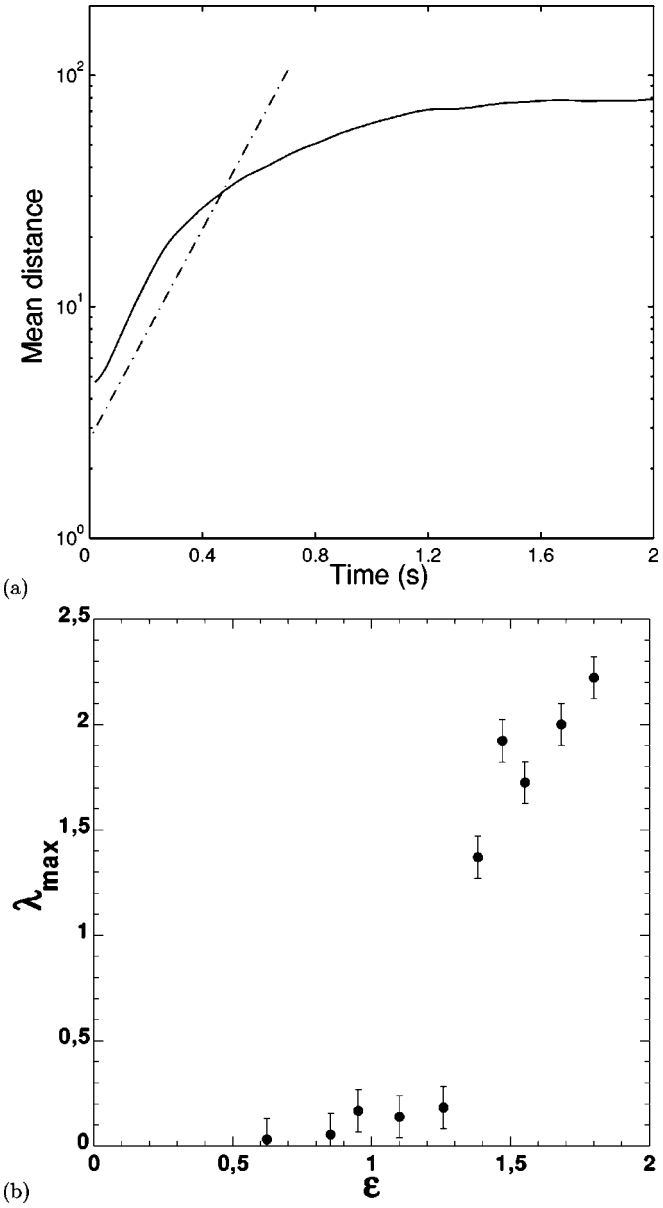

FIG. 6. (a) Example of the mean distance between two initially close points in the phase space, from which a Lyapunov exponent in extracted ($\epsilon = 1.67$). The dot-dashed line stands for the best fit of the initial exponential growth. (b) Maximal Lyapunov exponent vs distance to the threshold.

IV. FEEDBACK CONTROL OF OSCILLATORY INSTABILITY

The first problem to tackle in order to achieve a suitable control, is to determine the relative position of sensors and heaters that give the best efficiency. This is done with the help of the available information for the flow structure, dominated by a mode-2, and considering the following conditions:

- The positions of the two sensors have to enable the most complete information of the flow, and for that reason they are positioned in phase opposition with respect to each other (i.e., with a relative angle of $\pi/2$).
- The positions of the two heaters have to allow a "destructive" feedback to the dominant spatial mode-2. Thus, the heaters are located in phase in the spatial mode, i.e., with a relative angle of π. Each of them has a relative angle of $\pi/4$ with its respective sensor.

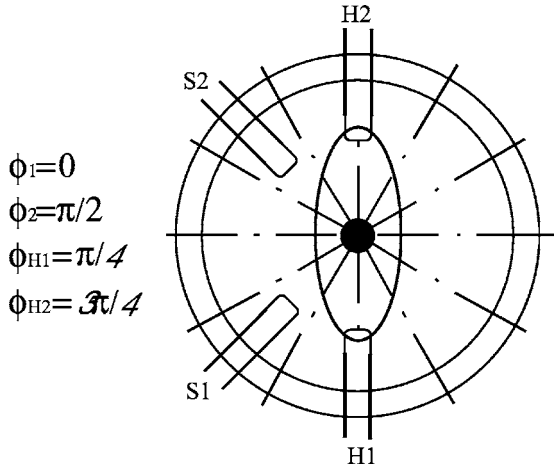

FIG. 7. Optimal disposition of sensors and heaters. The black solid circle, the concentric circles, and the ellipse represent the central cooling pipe, the heating ring at the periphery, and the structure of the dominant mode, respectively.

The chosen configuration is shown in Fig. 7, where the dominant mode is schematized by an ellipse, the center of the cell by a black solid circle, and the periphery of the cell by two concentric circles. Beyond these qualitative arguments, this optimization is the result of numerous attempts with various configurations.

As already mentioned in the setup description, the control is achieved in the following way. Defining $\theta(\phi_i)$ as the temperature difference measured by the sensor i and its temporal mean value $[\theta=(T-\bar{T})/\Delta T_c]$, one obtains the voltage injected to the heater i of resistance R_i (i equals 1 or 2) by the following law:

$$S = -G_1\theta(\Phi_i) - G_3\theta(\Phi_i)[\theta(\Phi_1)^2 + \theta(\Phi_2)^2],$$

$$V_i^2/R_i = S \quad \text{if } S > 0, \tag{3}$$

$$V_i = 0 \quad \text{if } S < 0.$$

Thus, if the temperature is lower than its temporal mean value $\bar{T}$, heating is applied by the corresponding heater. On the contrary, when it is higher than the mean value, no power is injected, as no local cooling can be brought by heaters. The injected power, given by V_i^2/R_i (R_i being the resistance of the heater), is of order of magnitude of a few tenths of a milliwatt. Equation (3) is a control-law combining a linear term, and a nonlinear term coupling the temperatures of both sensors to the third power. Appropriate choices for G_1 and G_3 are obtained by successive tries.

Illustrations of successful control are shown in Fig. 8 showing successively the time signals, the frequency power spectra and the Poincaré maps of both uncontrolled (dashed lines) and controlled (solid lines) states, for two values of ϵ: $\epsilon=0.24$ (a) and $\epsilon=0.72$. The Poincaré maps of Fig. 8 and of further figures have been obtained like in Fig. 5, but with a

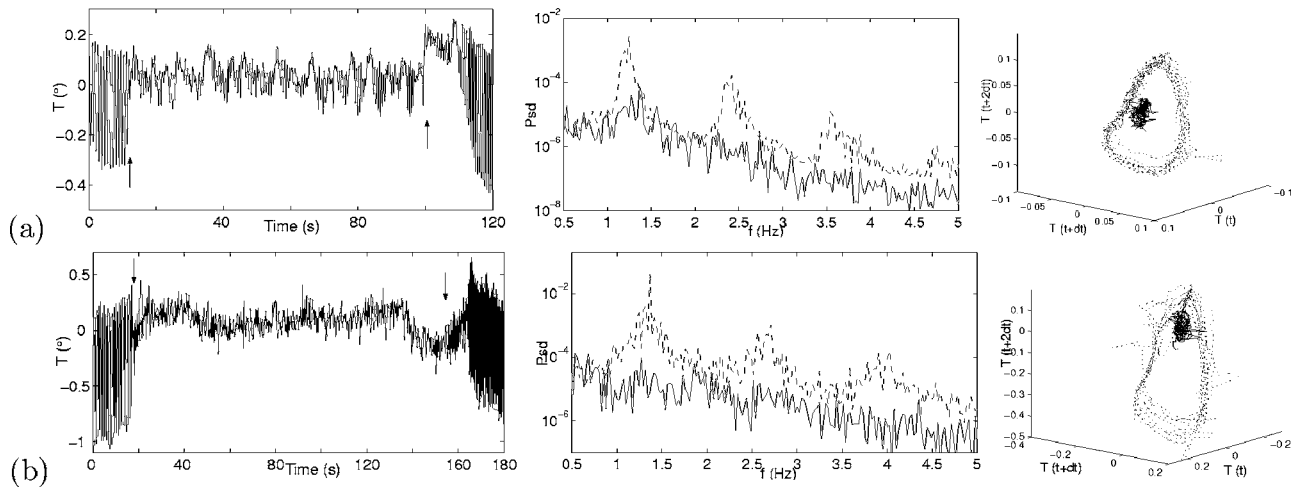

FIG. 8. Control of oscillatory instabilities. Time signal, the control is applied during the time between the two arrows—frequency spectra of both uncontrolled (dashed line) and controlled (solid line) states—Poincaré map of uncontrolled (dotted line) and controlled (solid line) states (time step 1/50 s). (a) $\epsilon=0.24$ and (b) $\epsilon=0.72$.

time step of 1/50 s. Obviously, applying control reduces significantly the amplitude of temperature fluctuations in both sensors. Not only the oscillations are damped, but also the controlled signal does not have any dominant frequency, presumably as a result of a destructive feedback on the initial dominant mode. It is worth mentioning that when the controlled signals from sensors 1 and 2 have different amplitudes, data are then not taken into account. For a more complete description of the flow under control, a recent numerical study has been achieved in a similar geometry.[23] Such a complete information of the flow under control was not possible to obtain experimentally: the light-reflective flakes would damage the thin fragile sensors and heaters. Figure 9(a) shows the injected power, corresponding to the case of Fig. 8(b), evidencing that power is kept very small (less than 1 mW) during the control. A slight burst is always observed in the very first stage of the control. Figures 9(b) and 9(c) represent a magnified view of (a), relating more clearly the instantaneous injected power and the temperature fluctuations measured by one sensor. These plots show that when T is lower than its current mean value, some heat is applied, unless the contribution of the nonlinear term (that couples the two sensors measurements) counterbalances the effect of the linear term.

Figures 10(a) and 10(b) are plots of the power of temperature signal of both uncontrolled and controlled states, the latter being obtained at control optimum. γ_{opt} is defined as the ratio in power between the controlled state and the uncontrolled one. The values of power are obtained by a numerical integration of the power spectra, in the frequency (f) range of 0.5 and 5 Hz. Defining Psd_{uc} and Psd_{c} as the power spectra of the uncontrolled and controlled signals of temperature, one gets

$$\gamma_{\mathrm{opt}} = \frac{\int_{0.5}^{5} \mathrm{Psd}_{c}(f)df}{\int_{0.5}^{5} \mathrm{Psd}_{uc}(f)df}.$$

The frequency boundaries are chosen to reject both slow fluctuations of temperature and very rapid fluctuations from the calculation, which are physically not relevant and which anyway do not contribute significantly to the power. The

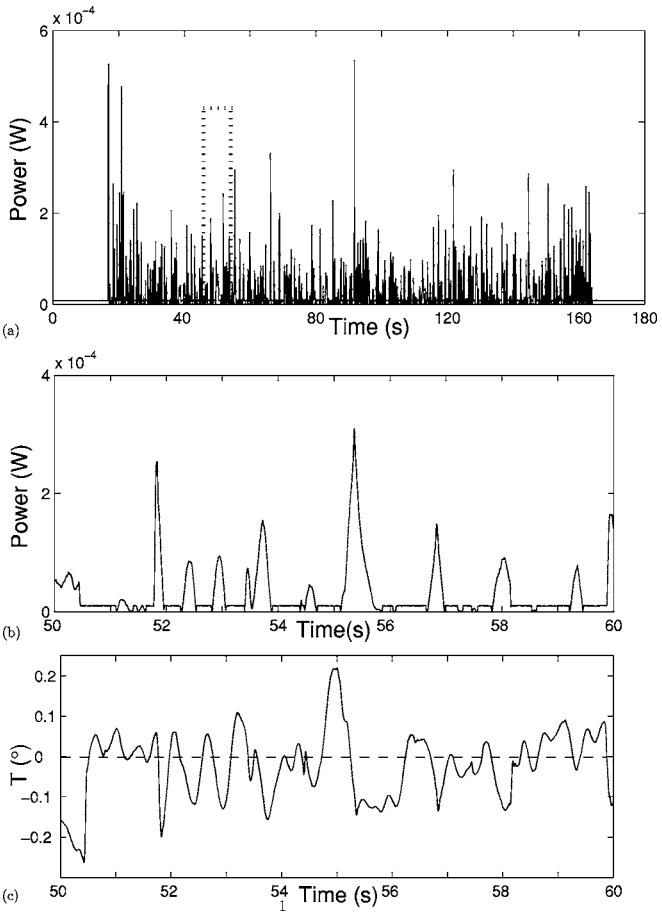

FIG. 9. (a) Power injected by a heater [the corresponding time signal is the one on Fig. 8(b)]. $\epsilon=0.72$. (b) and (c) Magnified view inside the time-zone defined in (a): power (injected by heater 1) and local temperature (measured on sensor 1). $G_1=3$ and $G_3=20$.

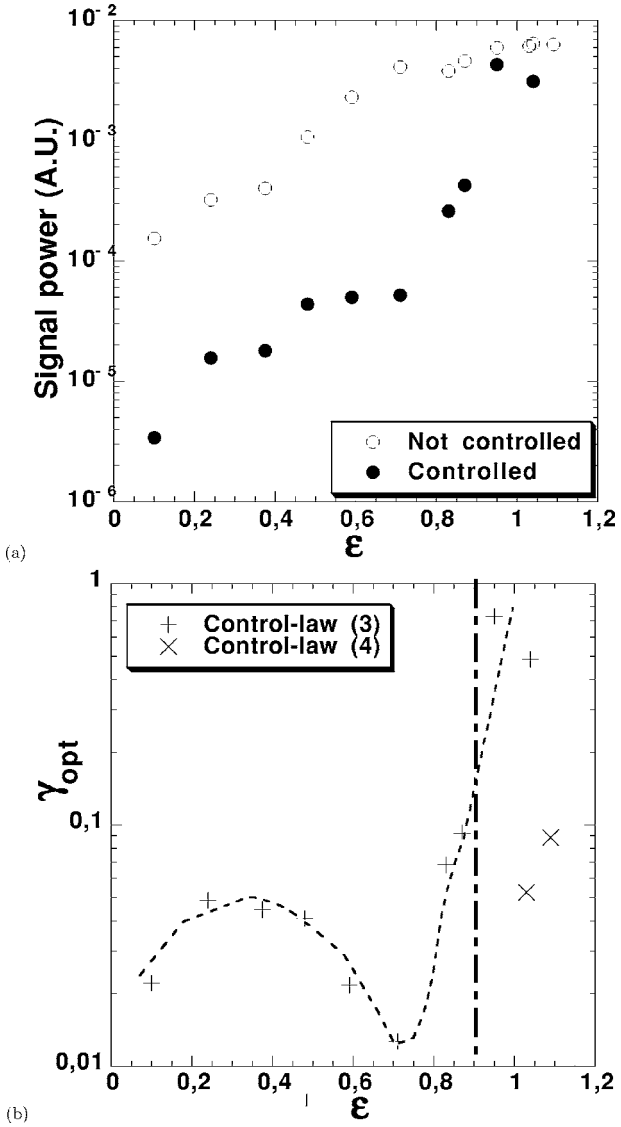

FIG. 10. (a) Power of temperature signal with and without control and (b) ratio of uncontrolled and controlled signals, for two different control laws (see the text for details). The vertical line stands for the value of ϵ, above which a purely proportional control is no longer efficient.

power is expressed in arbitrary units (square of temperature), as the relevant quantity to measure control efficiency is the ratio between power values. These plots show the following:

- From ϵ=0.2–0.75, the control efficiency is increasing, keeping values of γ_{opt} lower than 0.05 (corresponding to a ratio of peak-to-peak temperature fluctuations of order one-seventh).
- For ϵ larger than 0.75, the control starts to lose its efficiency, but is still satisfactory until approximately 0.9. Beyond 0.9, it was found that the control does not reduce the amplitude more than two-thirds.

Let us now focus on the values of coefficients G_1 and G_3 for optimum in Eq. (3). Figure 11 is particularly instructive about the progressive evolution of the relative weight of linear and nonlinear terms. It shows the evolution of the ratio between G_3 and G_1 for the best conditions of control. Obviously, the contribution of the nonlinear term becomes more

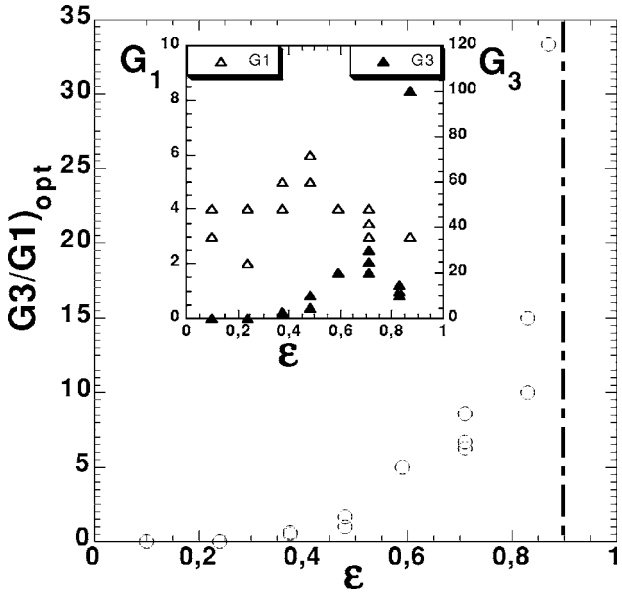

FIG. 11. Ratio between nonlinear and linear coefficients in the feedback control law, for the most efficient control. Insert: absolute values for G1 and G3, corresponding to conditions of best control performances.

and more important as ϵ increases. From some theoretical attempts[14] as well as experimental studies,[13] it is known that a simple linear control law is sufficient to attenuate the instabilities close to the oscillatory threshold. Our measurements show that when ϵ reaches approximately 0.4, the linear scheme (G_3=0) is not sufficient, presumably because nonlinear properties of the flow become predominant. In a similar system,[19] it has been shown that the contribution of the nonlinear cubic term had an effect on the order of the bifurcation to oscillating states, turning it from subcritical to supercritical. Thus, a nonzero value for G_3 should broaden the basin of attraction of the stabilized state, in order to make it possible the control of larger disturbances that occur at large ϵ. Otherwise, the increasing value of G_3 may reflect that it is more and more necessary to take into account temperature variations that occur at a certain distance from the operating heater, in order to anticipate eventual large fluctuations. A divergence of this ratio clearly appears around ϵ =0.9, i.e., near the threshold value for the occurrence of period-doubling secondary instability. This suggests that beyond a certain value of ϵ, a more complex law is needed to achieve control. This is exposed in the next section.

V. BEYOND PROPORTIONAL FEEDBACK: COMBINATION WITH A DERIVATIVE CONTROL LAW

Beyond a certain threshold ϵ, approximately equal to 0.9, it turns out that the feedback control obeying Eq. (3) could not achieve any attenuation of the temperature fluctuations. If the injected power is too weak, the system does not respond to the control whereas at stronger feedback power, the system exhibits sudden high-amplitude peaks of an amplitude up to 3 °C. In between, the control with appropriate choice for (G_1, G_3) is found to lead only to a slight decrease of fluctuations, showing occurrences of brief bursts. A careful observation of the time signals reveals that in fact, these

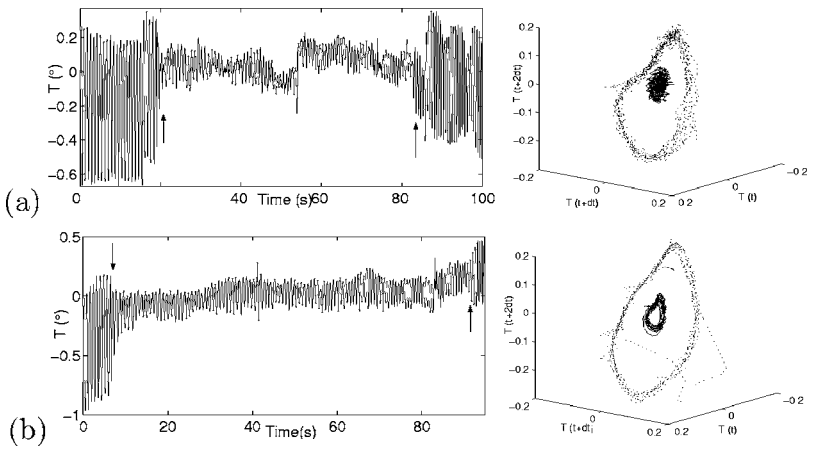

FIG. 12. Comparison between (a) PROP and (b) PROP+DER control laws for the same $\Delta T=27.0°$ (for legend explanation, see Fig. 8). $\epsilon=0.59$.

violent peaks come from a kind of resonance phenomenon arising in this range of parameters. To be more precise, when the signal is lower than its mean value, the control law of Eq. (3) imposes power injection. As the signal is already in a sharp increasing phase, the flow reacts unstably by naturally amplifying the feedback power. A remedy is to use another feedback law, combining proportional and derivative terms. Thus, the power injected by heaters will be lower if the time derivative of the signal is already positive and that the signal is about to overcome its mean value by the dynamics of the system itself. Also, when the signal is higher than its mean value, but strongly decreases, heating should be applied. The addition of a derivative term can then be seen as a way to anticipate the sudden variations. The control is then applied by a law such as

$$S = -G_1\left(\theta(\phi_i) + a\frac{\delta\theta(\phi_i)}{\delta t}\right),$$

$$V_i^2/R = S \quad \text{if } S > 0, \tag{4}$$

$$V_i = 0 \quad \text{if } S < 0,$$

where a is defined as the coefficient ruling the share between proportional (linear only) and derivative part. In all the measurements reported here, $a=10$. The derivative is calculated as the ratio between the temperature variation between two consecutive time steps, and the value of this time step δt (δt equals 1/50 s). Figures 12(a) and 12(b) illustrate control by purely proportional law (PROP) (a) and proportional +derivative (PROP+DER) law (b) for moderate ϵ. The performance of both methods are comparable, but at ϵ higher than 0.9, the PROP+DER method gives much better results, as shown in Fig. 13. As expressed in the previous part, the PROP law fails to control at high values of ϵ only contributing to a slight decrease of amplitude, whereas the PROP +DER law allows to pursue control at higher ϵ values. The limit of this control in terms of efficiency is determined to be around $\epsilon=1.15$. Two values of γ_{opt} are reported in Fig. 10(b) (time-cross symbols) showing a much better damping rate of power, lower than 0.1. The corresponding injected power of Fig. 13(b) is plotted on Fig. 14, showing that the heating is still bounded to small values (less than 1 mW).

About the suitable value of a around 10, it is worth underlining that it represents a time of 1/5 s (as the time step is 1/50 s). We tested lower and higher values for a, from 1 to 100. If $a=1$, nothing seems to be modified from the control given by Eq. (3), whereas if $a=50$ or 100, large bursts witness appearance of unstable phenomena. To be more precise, it turns out that a is the coefficient of the first-order derivative in the Taylor expansion of $\theta(\phi_i+a)$. The quantity a can be considered as a delay in both the phase variable and the real physical time (which are equivalent considering that the

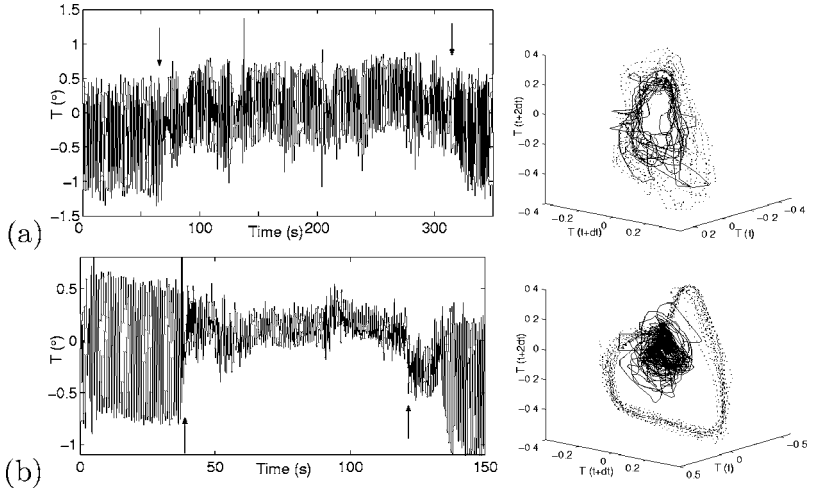

FIG. 13. Comparison between (a) PROP and (b) PROP+DER control laws for the same $\Delta T=34.6°$ [for legend explanation, see Fig. 8]. $\epsilon=1.03$.

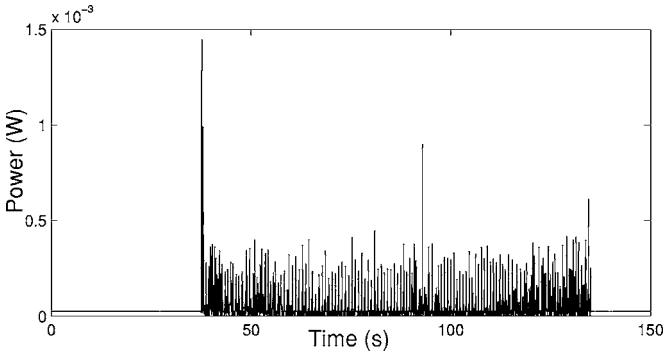

FIG. 14. Power injected by a heater [the corresponding time signal is the one on Fig. 13(b)]. $\epsilon=1.03$.

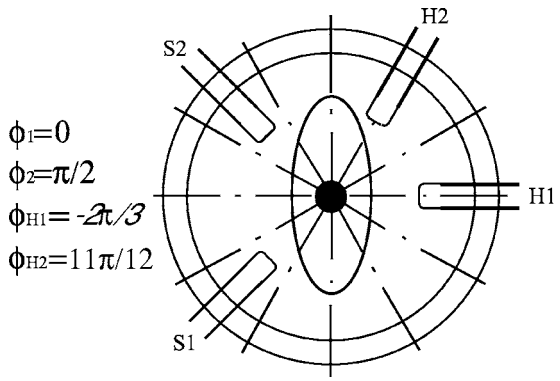

FIG. 15. Synchronization of chaos. (a) $\Delta T=43.1°$; $\epsilon=1.53$ and (b) $\Delta T=44,5°$; $\epsilon=1.62$.

dominant mode is still a traveling azimuthal wave). Then $a=10$ represents a suitable order of magnitude for this delay, in order to achieve the anticipation of sharp temperature variations.

VI. SYNCHRONIZATION OF CHAOS

When trying to apply the feedback control to a strongly chaotic state such as the one shown in Fig. 5(d), it turns out that no suitable feedback law such as (3) or (4), in any heater/sensor configuration, led to a significant attenuation of erratic fluctuations. However, it is possible to turn a chaotic state to a quasiperiodic state. Figures 15(a) and 15(b) are examples of such a synchronization.

The suitable heaters/sensors configuration is different from the one used previously: the sensors are still located at $\pi/2$ from one another, and the heaters are located at $\pi/3$ from one another. This is illustrated in Fig. 16. Further, it is worth noticing that the feedback law is purely proportional and fully linear [$G_3=0$ in (4)]. No efficient synchronization could be obtained by choosing a nonzero value for G_3. Looking at power spectra, it is remarkable that the dominant frequency of the controlled state is different from the initial one, and that the corresponding peak is sharper than the bump lying around the dominant frequency of the initial chaotic state. Although no direct visualization could be achieved during control (the seeding reflective particles would damage sensors), it is tempting to assume that this oscillatory state has a spatial structure different from the one dominating the initial chaotic state. This synchronization process could be interpreted as follows: the chaotic fluctuations of the initial state, still dominated by a spatial mode-2, are acquired in phase opposition (sensors at $\pi/2$ from each others) and reinjected similarly through the two heaters that will excite a mode of a different spatial structure (presumably spatial mode-3) which should be more stable than the mode-2 at this temperature difference. To achieve such a scenario, it is necessary to take some energy from the mode-2 and reinject it directly to the same phase shift of the mode-3, and then G_3 has obviously to be chosen equal to zero.

As shown in Fig. 15(b), the synchronization sometimes starts to be effective after a significant transient which can last more than 10 s, whereas for control of oscillatory states the decrease of amplitude is immediate. $\epsilon=1.62$ is close to the maximum value, for which such a synchronization is possible. Let us mention that if one determines the largest Lyapunov exponent of the uncontrolled and the controlled flows, by the same method as shown in Fig. 6, one finds a close-to-zero value for the controlled state, witnessing that the control *really* kills the unpredictable dynamics of the flow. The values of λ_{max} are 1.81 and 0.096 ($\epsilon=1.53$), and

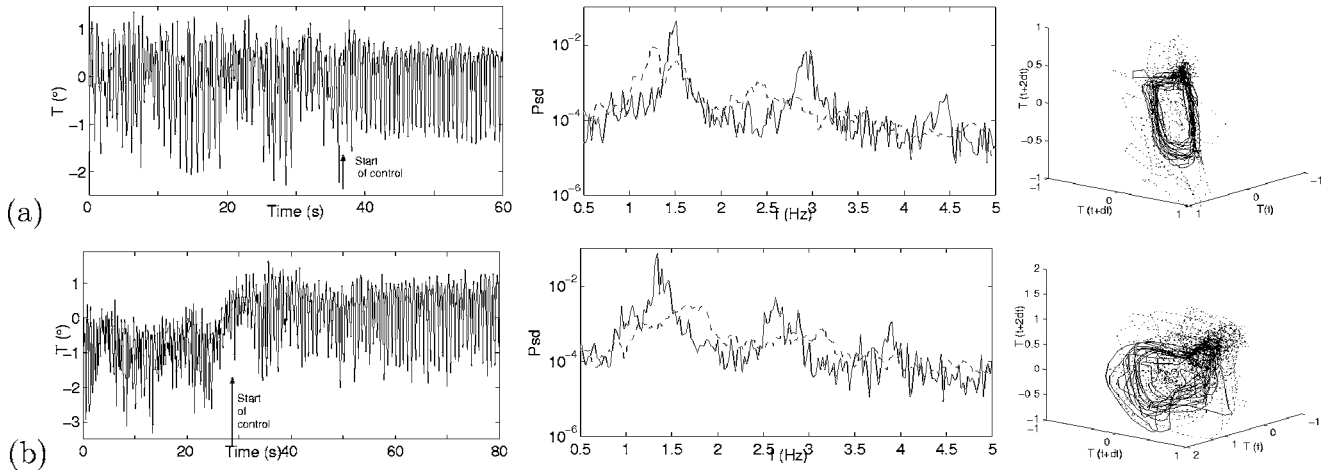

FIG. 16. Optimal disposition of sensors and heaters for synchronization of chaotic regimes.

1.88 and 0.11 ($\epsilon=1.62$), respectively, for the uncontrolled and the controlled state.

It also worth mentioning that several attempts were conducted by replacing in the control law the mean value of the signal $\bar{T}$ in the expression $\theta=(T-\bar{T})/\ \Delta T_c$), by the value of an oscillatory state of fixed amplitude and frequency, i.e., by replacing the distance from the mean value, by the "distance" of the temperature signal from a reference oscillatory state. No control nor synchronization of chaos could be obtained, for numerous combinations of sensor/heater configurations, amplitude and frequencies of the reference state.

VII. DISCUSSION AND CONCLUSIONS

To conclude, these results obtained on control of thermocapillary instabilities far from the stability threshold are significant and promising: to our knowledge, there are still few experimental examples of such control far from the threshold of the primary instability. Several points can be emphasized.

- This study presented different steps on unstable flow in a geometrically constrained annular thermocapillary driven flow. The choice of a flow converging from the periphery to the center, allowed to reach chaotic states similar to those obtained by Ueno *et al.*[9] in a half-zone liquid bridge. The dynamics is dominated by a spatial mode-2, which undergoes successive period-doubling bifurcations toward chaos as the driving force is increased. Chaotic behavior is evidenced by both smooth Fourier spectra and nonzero Lyapunov exponents.
- An active control of instabilities is achieved up to $\epsilon=1.05$, and the larger ϵ, the more complex the feedback law (i.e., far from a purely linear): nonlinear terms coupling the time signal measured on two locations as well as terms including the time-signal derivative are needed. This necessary complication of the feedback law could be seen as the first step towards an "optimal" control, theoretically described in Ref. 15 and named "OGY" from the authors' names.
- A synchronization of chaotic regimes could be achieved by the following way: by "pumping" the energy of the unstable dominant mode, and injecting it elsewhere in the cell to excite a different, more stable, spatial mode.

ACKNOWLEDGMENTS

The authors would like to thank J. Shiomi for helpful assistance in practical setup and theoretical advises. One of the authors (P.B.) would like to acknowledge the French foreign office for funding his year of postdoctoral study with a Lavoisier fellowship.

[1] J. M. Burgess, A. Juel, W. D. McCornick, J. B. Swift, and H. Swinney, "Suppression of dripping from a ceiling," Phys. Rev. Lett. **86**, 1203 (2001).
[2] S. H. Davis, "Thermocapillary instabilities," Annu. Rev. Fluid Mech. **19**, 403 (1987).
[3] Y. Kamotani, J. H. Lee, S. Ostrach, and A. Pline, "An experimental study of oscillatory thermocapillary convection in cylindrical container," Phys. Fluids A **4**, 955 (1992).
[4] T. Ondarcuhu, J. Millan-Rodriguez, H. L. Mancini, A. Garciamartin, and C. Perez-Garcia, "Bénard-Marangoni convective patterns in small cylindrical layers," Phys. Rev. E **48**, 1051 (1993).
[5] E. L. Koschmieder and S. A. Prahl, "Surface-tension driven Bénard convection in small containers," J. Fluid Mech. **215**, 571 (1990).
[6] A. B. Ezersky, A. Garciamartin, J. Burguete, H. L. Mancini, and C. Perez-Garcia, "Hydrothermal waves in Marangoni convection in a cylindrical container," Phys. Rev. E **47**, 1126 (1993).
[7] M. Jurisch, "Surface temperature oscillations of a floating zone resulting from oscillatory thermocapillary convection," J. Cryst. Growth **102**, 223 (1990).
[8] S. Frank and D. Schwabe, "Temporal and spatial elements of thermocapillary convection in floating zones," Exp. Fluids **23**, 234 (1997).
[9] I. Ueno, S. Tanaka, and H. Kawamura, "Oscillatory and chaotic thermocapillary convection in a half-zone liquid bridge," Phys. Fluids **15**, 408 (2003).
[10] J. Shiomi, M. Kudo, I. Ueno, H. Kawamura, and G. Amberg, "Feedback control of oscillatory thermocapillary convection in a half-zone liquid bridge," J. Fluid Mech. **496**, 193 (2003).
[11] D. Schwabe and S. Benz, "Thermocapillary flow instabilities in an annulus under microgravity-Results of the experiment Magia," Adv. Space Res. **29**, 629 (2002).
[12] Y. Kamotani, S. Ostrach, and J. Masud, "Microgravity experiments and analysis of oscillatory thermocapillary flows in cylindrical containers," J. Fluid Mech. **410**, 211 (2000).
[13] J. Shiomi and G. Amberg, "Active control of global thermocapillary convection," Phys. Fluids **14**, 3039 (2002).
[14] V. Petrov, M. F. Schatz, K. A. Muehlner, S. J. VanHook, W. D. McCormick, J. B. Swift, and H. Swinney, "Nonlinear control of remote unstable states in a liquid bridge convection experiment," Phys. Rev. Lett. **77**, 3779 (1996).
[15] J. Singer and H. H. Bau, "Active control of convection," Phys. Fluids A **3**, 2859 (1991).
[16] Y. Wang, J. Singer, and H. H. Bau, "Controlling chaos in a thermal convection loop," J. Fluid Mech. **237**, 479 (1992).
[17] P. K. Yuen and H. H. Bau, "Rendering a subcritical Hopf bifurcation supercritical," J. Fluid Mech. **317**, 91 (1996).
[18] H. H. Bau, "Control of Marangoni-Bénard convection," Int. J. Heat Mass Transfer **42**, 1327 (1999).
[19] A. C. Or and R. E. Kelly, "Feedback control of weakly nonlinear Rayleigh-Bénard-Marangoni convection," J. Fluid Mech. **440**, 27 (2001).
[20] P. Bergé, Y. Pomeau, and C. Vidal, *Order within Chaos: Towards a Deterministic Approach to Turbulence* (Wiley, New York 1987).
[21] E. Ott, C. Grebogi, and J. A. Yorke, "Controlling chaos," Phys. Rev. Lett. **64**, 1196 (1990).
[22] H. Kantz, "A robust method to estimate the maximal Lyapunov exponent of a time series," Phys. Lett. A **185**, 77 (1994).
[23] J. Shiomi and G. Amberg, "Numerical investigation of feedback control of thermocapillary instability," Phys. Fluids **17**, 054107 (2005).